

Electronic Supplementary Information (ESI)

Aliovalent-cation-substitution-induced structure transformation: a new path toward high-performance IR nonlinear optical materials

Chang Liu,^{‡a} Sheng-Hua Zhou,^{‡b,c} Yu Xiao,^d Chao Zhang,^d Hua Lin,^{*,b,e} and Yi Liu^{*,d}

^aSchool of Materials Science and Engineering, Shaanxi University of Science and Technology, Xi'an 710021, China

^bState Key Laboratory of Structural Chemistry, Fujian Institute of Research on the Structure of Matter, Chinese Academy of Sciences, Fuzhou 350002, China

^cUniversity of Chinese Academy of Sciences, Beijing 100049, China

^dInstitute for Composites Science Innovation, School of Materials Science and Engineering, Zhejiang University, Hangzhou 310027, China

^eFujian Science & Technology Innovation Laboratory for Optoelectronic Information of China, Fuzhou, Fujian 350108, China

[‡]C. Liu and S. H. Zhou contributed equally to this work.

**E-mail: liuyimse@zju.edu.cn and linhua@fjirsm.ac.cn.*

Electronic Supplementary Information Index

1. Experimental Section

1.1 Materials and Instruments

1.2 Synthesis

1.3 Second-Harmonic Generation (SHG) Measurements

1.4 Laser Induced Damage Threshold (LIDT) Measurements

1.5 Single-Crystal Structure Characterizations

2. Computational Details

3. Figures and Tables

Figure S1. (a) One-dimensional $_{\infty}[\text{Ag}_3\text{S}_5]^{7-}$ chain in the structure of $\text{K}_2\text{Ag}_3\text{Sb}_3\text{S}_7$ and (b) the local coordination environment of the Ag atoms with atomic numbers outlined.

Figure S2. The local coordination environment of the K atoms in the structure of (a) NCS $\text{K}_2\text{Ag}_3\text{Sb}_3\text{S}_7$ and CS $\text{K}_2\text{Sb}_4\text{S}_7$.

Figure S3. The experimental (blue) and simulated (black) powder XRD of (a) $\text{K}_2\text{Ag}_3\text{Sb}_3\text{S}_7$.

Figure S4. EDX results and the obtained compositions of $\text{K}_2\text{Ag}_3\text{Sb}_3\text{S}_7$.

Figure S5. The first Brillouin zone with high symmetry points of $\text{K}_2\text{Ag}_3\text{Sb}_3\text{S}_7$.

Table S1 Crystallographic data and refinement details for $\text{K}_2\text{Ag}_3\text{Sb}_3\text{S}_7$.

Table S2 Atomic coordinates and equivalent isotropic displacement parameters of $\text{K}_2\text{Ag}_3\text{Sb}_3\text{S}_7$.

Table S3 Selected bond lengths (\AA) and angle ($^{\circ}$) of $\text{K}_2\text{Ag}_3\text{Sb}_3\text{S}_7$.

4. References

1. Experimental Section

1.1 Materials and Instruments

All reagents used in the present experiments were purchased from commercial sources and directly used without further purification. The optical diffuse reflectance spectra were performed on a Perkin-Elmer Lambda 900 UV–vis-NIR spectrometer equipped with an integrating sphere at room temperature. BaSO₄ was used as 100 % reflectance reference, and the polycrystalline samples were prepared by grinding single crystals into fine powder before the measurements. The absorption (α/S) data were converted from diffuse reflectance spectra using the Kubelka–Munk function: $\alpha/S = (1-R)^2/2R$, in which R is the reflectance at a given wavelength, α is the absorption coefficient, and S is the scattering coefficient.¹ The elemental analyses were examined with the aid of an EDX-equipped JEOL/JSM-6360A SEM. Powder X-ray diffraction (PXRD) analysis was carried out in a Rigaku Mini-Flex 600 powder diffractometer (Cu-K α , $\lambda = 1.5418 \text{ \AA}$).

1.2 Synthesis

All chemical reagents used in the present experiments were commercially available, no further purification were performed. Yellow crystals of K₂Ag₃Sb₃S₇ were synthesized by the following reactions: 2.0 mmol of KOH, 1.0 mmol of Ag, 0.5 mmol of Sb₂S₃, 2.0 mmol of S, 1.0 mL of N₂H₄·H₂O and 2.0 mL PEG-400 were mixed together and sealed in a 25 mL Teflon-lined stainless autoclave and heated at 433 K for 7 days. The resultant reaction mixtures were washed with deionized water and ethanol, respectively, and the yield is about 80% (based on Ag).

1.3 Second-Harmonic Generation (SHG) Measurements

The powder SHG measurements were carried out with the Kurtz-Perry method using a 2050 nm Q-switch laser.² AgGaS₂ was used as a benchmark material, which is provided by Anhui Institute of Optics and Fine Mechanics, Chinese Academy of Sciences. K₂Ag₃Sb₃S₇ and AgGaS₂ were ground and sieved into distinct particle size ranges (30–46, 46–74, 74–106, 106–150, 150–210 μm). The SHG signals of the frequency-doubled output emitted from the sieved samples were detected using a photomultiplier tube and recorded on the oscilloscope.

1.4 Laser Induced Damage Threshold (LIDT) Measurements

The LIDT of K₂Ag₃Sb₃S₇ at the range of 150–210 μm was measured through single pulse measurement method³ and crushed AgGaS₂ single crystal as the reference. Both samples were packed into identical plastic holders (thickness: 1 mm and diameter: 8 mm). After being exposed to the high-power 1064 nm laser radiation with pulse width τ_p of 10 ns, the apparent change of sample was monitored by an optical microscope. The power of laser beam and the damage spot radius were respectively measured by a Nova II sensor with a PE50-DIF-C energy sensor and a Vernier caliper.

1.5 Single-Crystal Structure Characterizations

Room-temperature single-crystal XRD data were collected on an Oxford Xcalibur (Atlas Gemini ultra) diffractometer with a graphite-monochromated Mo-K_α radiation ($\lambda = 0.71073 \text{ \AA}$). The absorption correction was done by the multi-scan method.⁴ The direct methods was adopted to solve the crystal structure, and refined by the full-matrix least-square fitting on F^2 using the *SHELX-2014* program package.⁵ The

Electronic Supplementary Information (ESI)

assignments of K, Ag, Sb, and S were determined on the basis of the interatomic distances and relative displacement parameters. All of the atoms were refined with anisotropic thermal parameters and a secondary extinction correction. The final atomic positions were standardized with the *Structure Tidy* program.⁶ Note that the Ag2 atom was refined as split site (e.g., Ag2A, and Ag2B) due to the high atomic displacement parameter and the occupancies were refined to 85%, and 15%, respectively. Crystallographic information and selected bond distances for the title compound are summarized in Tables S1–3. CCDC number: 2105044.

2. Computational Details

The DFT calculations have been performed using the *Vienna ab initio simulation package* (VASP)^{7–9} with the Perdew-Burke-Ernzerhof (PBE)¹⁰ exchange correlation functional. The projected augmented wave (PAW)¹⁰ potentials have been used. A Γ -centered $7 \times 7 \times 5$ Monkhorst-Pack grid for the Brillouin zone sampling¹² and a cutoff energy of 600 eV for the plane wave expansion were found to get convergent lattice parameters. Both the cell and atomic relaxations were carried out until the residual forces are below 0.02 eV/Å. A Monkhorst-Pack k -point mesh of $7 \times 9 \times 9$ was used for the calculation of the linear and nonlinear optical properties.

The imaginary part of the dielectric function due to direct inter-band transitions is given by the expression:

$$\varepsilon_2(\mathbf{h}\omega) = \frac{2e^2\pi}{\Omega\varepsilon_0} \sum_{k,v,c} \left| \langle \psi_k^c | \mathbf{u} \cdot \mathbf{r} | \psi_k^v \rangle \right|^2 \delta(E_k^c - E_k^v - E) \quad \dots\dots\dots (1)$$

where Ω , ω , u , v and c are the unit-cell volume, photon frequencies, the vector defining the polarization of the incident electric field, valence and conduction bands,

Electronic Supplementary Information (ESI)

respectively. The real part of the dielectric function is obtained from ε_2 by a Kramers-Kronig transformation:

$$\varepsilon_1(\omega) = 1 + \left(\frac{2}{\pi}\right) \int_0^{+\infty} d\omega' \frac{\omega'^2 \varepsilon_2(\omega')}{\omega'^2 - \omega^2} \dots\dots\dots (2)$$

The refractive index $n(\omega)$ can be obtained based on ε_1 and ε_2 .

In calculation of the static $\chi^{(2)}$ coefficients, the so-called length-gauge formalism derived by Aversa and Sipe¹³ and modified by Rashkeev et al¹⁴ is adopted, which has proven to be successful in calculating the second order susceptibility for semiconductors and insulators. In the static case, the imaginary part of the static second-order optical susceptibility can be expressed as:

$$\begin{aligned} \chi^{abc} &= \frac{e^3}{\hbar^2 \Omega} \sum_{nml,k} \frac{r_{nm}^a (r_{ml}^b r_{ln}^c + r_{ml}^c r_{ln}^b)}{2\omega_{nm} \omega_{ml} \omega_{ln}} [\omega_n f_{ml} + \omega_m f_{ln} + \omega_l f_{nm}] \\ &+ \frac{ie^3}{4\hbar^2 \Omega} \sum_{nm,k} \frac{f_{nm}}{\omega_{mn}^2} [r_{nm}^a (r_{mn;c}^b + r_{mn;b}^c) + r_{nm}^b (r_{mn;c}^a + r_{mn;a}^c) + r_{nm}^c (r_{mn;b}^a + r_{mn;a}^b)] \\ &\dots\dots\dots(3) \end{aligned}$$

where r is the position operator, $\hbar\omega_{nm} = \hbar\omega_n - \hbar\omega_m$ is the energy difference for the bands m and n , $f_{mn} = f_m - f_n$ is the difference of the Fermi distribution functions, subscripts a , b , and c are Cartesian indices, and $r_{mn;a}^b$ is the so-called generalized derivative of the coordinate operator in k space,

$$r_{nm;a}^b = \frac{r_{nm}^a \Delta_{mn}^b + r_{nm}^b \Delta_{mn}^a}{\omega_{nm}} + \frac{i}{\omega_{nm}} \times \sum_l (\omega_{lm} r_{nl}^a r_{lm}^b - \omega_{nl} r_{nl}^b r_{lm}^a) \dots\dots\dots (4)$$

where $\Delta_{nm}^a = (p_{nm}^a - p_{mm}^a) / m$ is the difference between the electronic velocities at the bands n and m .

As the nonlinear optical coefficients is sensitive to the momentum matrix, much

Electronic Supplementary Information (ESI)

finer k-point grid and large amount of empty bands are required to obtain a convergent $\chi^{(2)}$ coefficient. The $\chi^{(2)}$ coefficients here were calculated from PBE wave functions and a scissor operator has been added to correct the conduction band energy (corrected to the experimental gap), which has proven to be reliable in predicting the second order susceptibility for semiconductors and insulators.

3. Figures and Tables

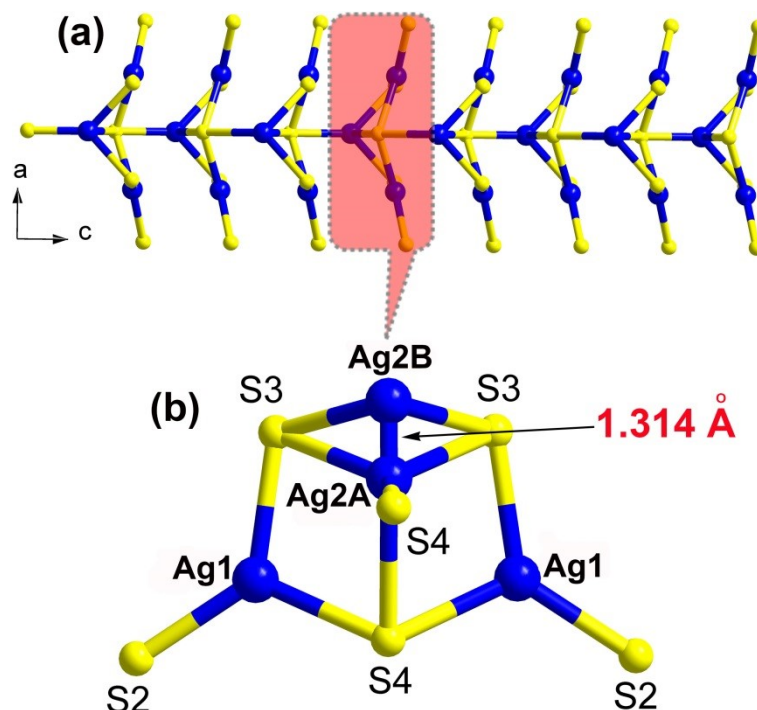


Figure S1. (a) One-dimensional $\infty[Ag_3S_5]^{7-}$ chain in the structure of $K_2Ag_3Sb_3S_7$ and (b) the local coordination environment of the Ag atoms with atomic numbers outlined.

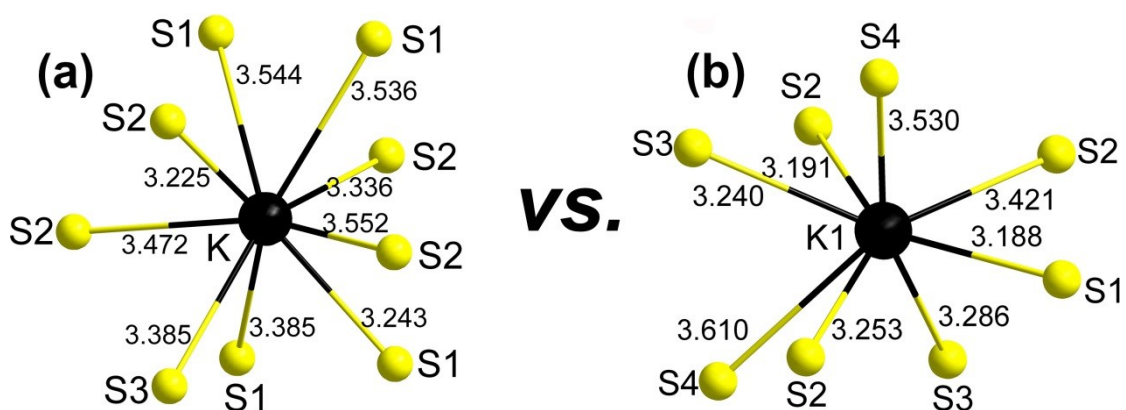


Figure S2. The local coordination environment of the K atoms in the structure of (a) NCS $K_2Ag_3Sb_3S_7$ and (b) CS $K_2Sb_4S_7$.

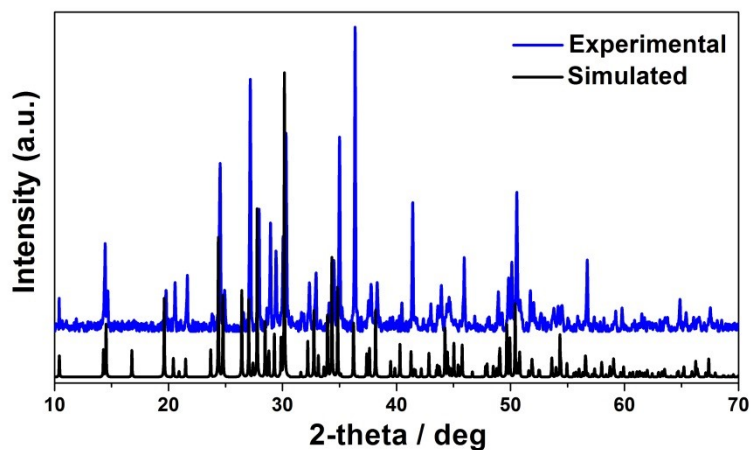


Figure S3. The experimental (blue) and simulated (black) powder XRD of (a) $K_2Ag_3Sb_3S_7$.

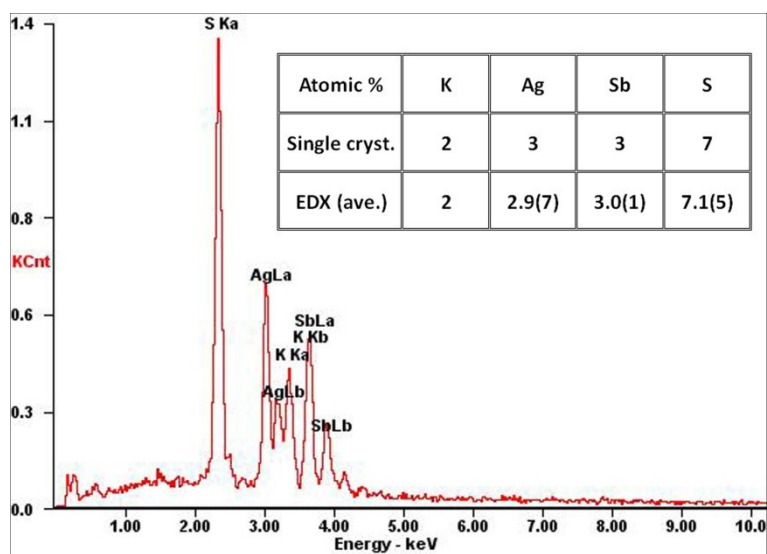


Figure S4. EDX results and the obtained compositions of $K_2Ag_3Sb_3S_7$.

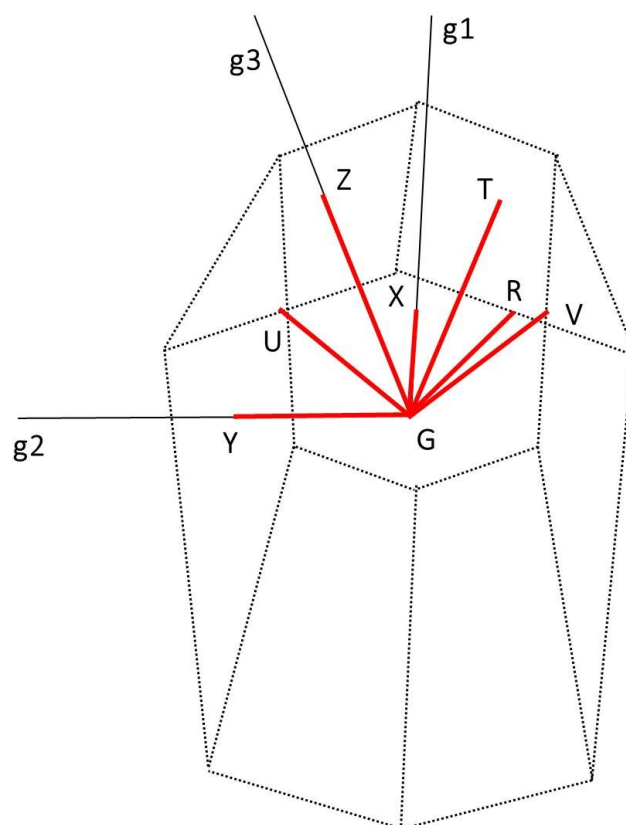


Figure S5. The first Brillouin zone with high symmetry points of $K_2Ag_3Sb_3S_7$.

Electronic Supplementary Information (ESI)

Table S1. Crystallographic data and refinement details for $K_2Ag_3Sb_3S_7$.

formula	$K_2Ag_3Sb_3S_7$
fw	991.48
crystal system	Orthorhombic
Temperature (K)	293
crystal color	Yellow
space group	$Cmc2_1$ (No.36)
a (Å)	24.836(8)
b (Å)	6.760(2)
c (Å)	11.52(2)
α (deg.)	90
β (deg.)	90
γ (deg.)	90
V (Å ³)	1519.2(8)
Z	4
D_c (g/cm ³)	4.335
μ (mm ⁻¹)	10.522
GOOF on F^2	1.141
R_1, wR_2 ($I > 2\sigma(I)$) ^a	0.0289, 0.0651
R_1, wR_2 (all data)	0.0293, 0.0653
largest diff. Peak / hole (e/Å ³)	1.242 / -0.932

$$^aR_1 = \frac{\sum ||F_o| - |F_c||}{\sum |F_o|}, wR_2 = [\frac{\sum w(F_o^2 - F_c^2)^2}{\sum w(F_o^2)^2}]^{1/2}$$

Electronic Supplementary Information (ESI)

Table S2. Atomic coordinates and equivalent isotropic displacement parameters of $\text{K}_2\text{Ag}_3\text{Sb}_3\text{S}_7$.

Atom	Wyckoff	<i>x</i>	<i>y</i>	<i>z</i>	$U_{(\text{eq})}^*$	Occu.
K	8 <i>b</i>	0.29267(11)	0.3106(3)	0.1851(5)	0.0291(6)	1.0
Ag1	8 <i>b</i>	0.41019(5)	0.50643(14)	0.1268(2)	0.0469(4)	1.0
Ag2A	4 <i>a</i>	0.5	0.3204(5)	0.8694(4)	0.0756(10)	0.85(3)
Ag2B	4 <i>a</i>	0.5	0.175(2)	0.872(2)	0.062(4)	0.15(3)
Sb1	8 <i>b</i>	0.37234(3)	0.88959(8)	0.18413(12)	0.0168(2)	1.0
Sb2	4 <i>a</i>	0.5	0.15662(13)	0.3293(2)	0.0243(3)	1.0
S1	8 <i>b</i>	0.31178(12)	1.0054(4)	0.4265(5)	0.0208(6)	1.0
S2	8 <i>b</i>	0.32873(12)	0.6529(3)	0.1913(6)	0.0245(7)	1.0
S3	8 <i>b</i>	0.42466(12)	0.2301(4)	0.1219(6)	0.0273(8)	1.0
S4	4 <i>a</i>	0.5	0.3786(8)	0.5266(10)	0.0441(16)	1.0

* $U_{(\text{eq})}$ is defined as one-third of the trace of the orthogonalized U_{ij} tensor.

Electronic Supplementary Information (ESI)

Table S3. Selected bond lengths (Å) and angles (°) of $A_3Mn_2Sb_3S_8$ ($A = K$ and Rb).

Ag1–S2	2.458(3)	Sb2–S4	2.411(6)
Ag1–S3	2.526(3)	Sb2–S3	2.431(3)
Ag1–S4	2.553(3)	Sb2–S3	2.431(3)
Ag2A–S4	2.377(8)	K–S2	3.225(4)
Ag2A–S3	2.661(4)	K–S1	3.243(5)
Ag2A–S3	2.661(4)	K–S2	3.336(4)
Ag2A–S4	2.924(8)	K–S1	3.385(5)
Ag2B–S3	2.569(10)	K–S3	3.385(4)
Ag2B–S3	2.569(10)	K–S2	3.472(5)
Sb1–S2	2.400(3)	K–S1	3.536(4)
Sb1–S1	2.459(3)	K–S1	3.544(4)
Sb1–S1	2.489(3)	K–S2	3.552(5)
<hr/>			
∠S2–Ag1–S3	130.79(11)	∠S2–Sb1–S1	95.21(12)
∠S2–Ag1–S4	123.12(17)	∠S2–Sb1–S1	94.71(12)
∠S3–Ag1–S4	106.00(17)	∠S1–Sb1–S1	86.21(8)
∠S4–Ag2–S3	133.89(10)	∠S3–Sb2–S3	95.23(15)
∠S4–Ag2–S3	133.89(10)	∠S2–Sb2–S3	95.23(15)
∠S3–Ag2–S3	89.37(17)	∠S5–Sb2–S3	100.65(18)
∠S4–Ag2–S4	98.5(2)		
∠S3–Ag2–S4	93.05(14)		
∠S3–Ag2–S4	93.05(14)		

4. References

1. P. Kubelka, An article on optics of paint layers, *Z. Tech. Phys.*, 1931, **12**, 593–601.
2. S. K. Kurtz and T. T. Perry, A powder technique for the evaluation of nonlinear optical materials, *J. Appl. Phys.*, 1968, **39**, 3798–3813.
3. M. J. Zhang, X. M. Jiang, L. J. Zhou and G. C. Guo, Two phases of Ga₂S₃: promising infrared second-order nonlinear optical materials with very high laser induced damage thresholds, *J. Mater. Chem. C*, 2013, **1**, 4754–4760.
4. *CrystalClear* Version 1.3.5; Rigaku Corp.: Woodlands, TX, 1999.
5. G. M. Sheldrick, A short history of SHELX, *Acta Crystallogr., Sect. A: Found. Crystallogr.* 2008, 112–122.
6. L. M. Gelato and E. J. Parthe, STRUCTURE TIDY—a computer program to standardize crystal structure data, *Appl. Crystallogr.* 1987, **20**, 139–143.
7. G. Kresse, VASP, 5.3.5; <http://cms.mpi.univie.ac.at/vasp/vasp/vasp.html>.
8. G. Kresse, J. Furthmuller, Efficient iterative schemes for ab initio total-energy calculations using a plane-wave basis set, *Phys. Rev. B: Condens. Matter*, 1996, 11169–11186.
9. G. Kresse and D. Joubert, From ultrasoft pseudopotentials to the projector augmented-wave method, *Phys. Rev. B: Condens. Matter*, 1999, **59**, 1758–1775.
10. P. E. Blochl, Projector augmented-wave method, *Phys. Rev. B: Condens. Matter*, 1994, **50**, 17953–17979.
11. J. P. Perdew, K. Burke and M. Ernzerhof, Generalized gradient approximation made simple, *Phys. Rev. Lett.*, 1996, **77**, 3865–3868.

Electronic Supplementary Information (ESI)

12. D. J. Chadi, Special points for Brillouin-zone integrations, *Phys. Rev. B: Condens. Matter*, 1976, **16**, 1746–1747.
13. C. Aversa and J. E. Nonlinear optical susceptibilities of semiconductors: Results with a length-gauge analysis, Sipe, *Phys. Rev. B*, 1995, **52**, 14636–14645.
14. S. N. Rashkeev, W. R. L. Lambrecht and B. Segall, Efficient ab initio method for the calculation of frequency-dependent second-order optical response in semiconductors, *Phys. Rev. B*, 1998, **57**, 3905–3919.